

We are IntechOpen, the world's leading publisher of Open Access books Built by scientists, for scientists

6,900

Open access books available

186,000

International authors and editors

200M

Downloads

Our authors are among the

154

Countries delivered to

TOP 1%

most cited scientists

12.2%

Contributors from top 500 universities



WEB OF SCIENCE™

Selection of our books indexed in the Book Citation Index
in Web of Science™ Core Collection (BKCI)

Interested in publishing with us?
Contact book.department@intechopen.com

Numbers displayed above are based on latest data collected.
For more information visit www.intechopen.com



Fabrication and Characterization of MicroPCMs

Jun-Feng Su

*Institute of Materials Science and Chemical Engineering,
Tianjin University of Commerce,
P. R. China*

1. Introduction

The increasing gap between the demand and supply of energy is an essential problem affecting the globe climate and economy. Energy efficiency improvement is one approach to reduce the mismatch between supply and demand. Energy conservation can be achieved through increased efficient energy use, in conjunction with decreased energy consumption and/or reduced consumption from conventional energy sources. Thermal energy conservation is easy to realize by storing thermal energy as latent heat in which energy is stored when a substance changes from one phase to another by either melting or freezing. The temperature of the substance remains constant during phase change. Phase change materials (PCMs) include organic (e. g. paraffin), inorganic (e. g. salt hydrates) and salt eutectics (e. g. $\text{CaCl}_2 \cdot \text{MgCl}_2 \cdot \text{H}_2\text{O}$) have been widely studied and applied in energy saving field. A good design for the PCMs requires that their phase-change processes, especially the melting and solidification processes perform in a container. It is also proposed that the heat transfer rate between PCM and source/sink can be increased by using microencapsulated PCMs (microPCMs). The reason is that the small microPCMs provide larger heat transfer area per unit volume and thus higher heat transfer rate. Moreover, the microPCMs bring in more advantages like less reaction of PCM with matrix material, ability to withstand volume change during phase change, etc.

To date, microPCMs have two application approaches: in emulsion and in solid matrix. Emulsion containing microPCMs can be used as thermal exchange medium to enhance the energy efficiency of thermal exchanger. MicroPCMs are widely applied in solid matrix as smart thermal-regulation composites, such as fibers, construction materials, blood temperature-controlling materials and anti-icing coats.

This chapter summarized our published works on fabrication and characterization of microPCMs, including shell compactability enhancement, thermal and chemical stability improvement, heat conductivity accelerating and phase change behavior controlling. Styrene-maleic anhydride (SMA) copolymer solid was used as a nonionic dispersant. These microPCMs have been applied in energy saving fields.

In addition, the strength of the bond at the microcapsule/matrix interface controls the fatigue life of the composites significantly. So by controlling the stress-strain response and ductility of the interface region, it is possible to control overall behavior of the composites. We applied a methanol-modified process to enhance the banding of microPCMs and the

polymer matrix. The interface morphologies were investigated systemically to understand the effects of the average diameters, contents and core/shell ratios of microPCMs on the interface stability behaviors.

2. Fabrication and characterization MF-shell microPCMs

Melamine-formaldehyde (MF) resin [1, 2], urea-formaldehyde (UF) resin [3, 4] and polyurethane (PU) [5-7] were usually selected as microcapsule shell materials for the PCMs protection. In practical usages of microPCMs, the volume of PCM in shells will change obviously during absorbing and releasing thermal energy. The volume alternant changes original bring the liquefied PCMs leaking from the microcapsules. And the breakage of the shell will happen based on the mismatch of thermal expansion of the core and shell materials at high temperatures [5]. Thus, it is necessary to keep the shell stability and compact for a long-life with less cracks and lower permeability.

MF resin has been successfully applied as shell material of microcapsules in fields of carbonless copying paper, functional textiles, liquid crystals, adhesives, insecticides and cosmetics [8]. Furthermore, literatures have showed that MF has been applied for microPCMs encapsulating various solid-liquid PCMs with the size range of about 50 nm to 2 mm. Generally, MF resin is adsorbed and cured on surfaces of core particles though an in-suit polymerization with the help of a polymeric surfactant.

2.1 Materials and fabrication method

Styrene maleic anhydride copolymer solid (SMA, Scripset®520, Hercules, USA) was used as a dispersant. A small percentage of the anhydride groups have been established with a low molecular weight alcohol and it is fine, off-white, free flowing powder with a faint, aromatic odor. Nonionic surfactant, NP-10 [poly (ethylene glycol) nonylphenyl] getting from Sigma Chemical was used as an emulsifier. The pre-polymer of melamine-formaldehyde (MF) resin which solid content was 50±2wt. %, was purchased from Shanghai Hongqi. Chem. Company (Shanghai, China). The *n*-octadecane purchased from Tianjin Fine Chemical Company (Tianjin, China) was encapsulated as the core material. All other chemical reagents were analytical purity and supplied by Tianjin Kermel Chemical Reagent Development Center (Tianjin, China).

Microcapsulation by coacervation proceeds along three main steps:

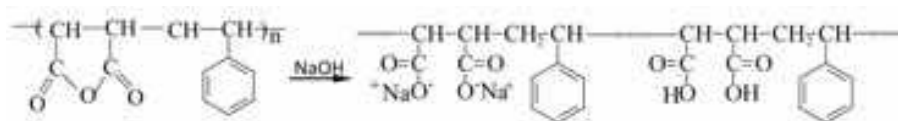
1. Phase separation of the coating polymer solution. SMA (10.0 g) and NP-10 (0.2 g) were added to 100 ml water at 50 °C and allowed stir for 20 min. And then a solution of NaOH (10%) was added dropwise adjusting its pH value to 4-5. The above surfactant solution and *n*-octadecane (32 g) were emulsified mechanically under a vigorous stirring rate of 3000 r min⁻¹ for 10 min using a QSL high-speed disperse-machine (Shanghai Hongtai Ltd, Shanghai, China.).
2. Adsorption of the coacervation around the core particles. The encapsulation was carried out in a 500 ml three-neck round-bottomed flask equipped with a condenser and a tetrafluoroethylene mechanical stirrer. The above emulsion was transferred in the bottle, which was dipped in steady temperature flume. Half of MF pre-polymer (16 g) was added dropwise with a stirring speed of 1500 r·min⁻¹. After 1h, the temperature was increased to 60 °C with a rate of 2 °C·min⁻¹. Then another half of pre-polymer (16 g) was dropped in bottle at the same dropping rate.

- Solidification of the microparticles. Then the temperature was increased to 75 °C. After polymerization for 1h, the temperature was decreased slowly at a rate of 2 °C·min⁻¹ to atmospheric temperature.

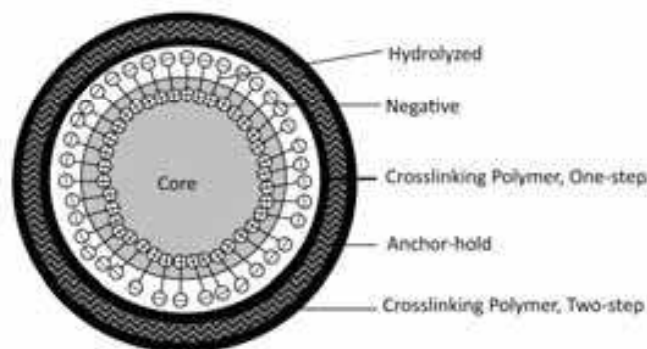
At last, the resultant microcapsules were filtered and washed with pure water and dried in a vacuum oven. In addition, we could control the average diameter of microcapsules by stirring speed. Also, the OSC microPCMs was fabricated in this work according to the above process by adding the same amount (32 g) prepolymer shell material in one step.

2.2 Mechanism of TSC

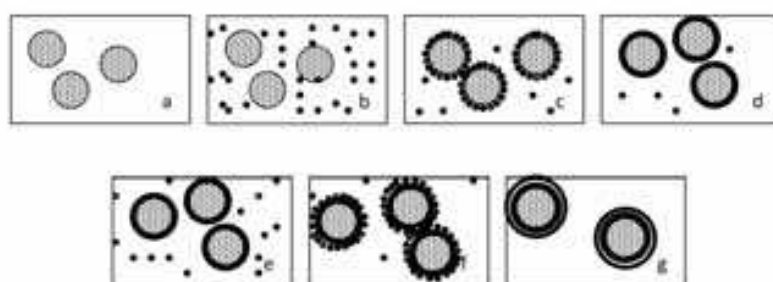
Hydrolyzed SMA is a kind of polymeric surfactant that is soluble in water but sufficiently amphiphilic to be absorbed by surfaces and interfaces, particularly by dispersed solid or liquid phases [9]. In addition, hydrolyzed SMA plays two important roles during the formation of microcapsules: dispersant and anionic polyelectrolyte [10, 11].



(a)



(b)



(c)

Fig. 1. Sketch mechanism of the fabrication process to TSC microcapsules: (a) Chemical structures of styrene maleic anhydride (SMA) alternating copolymer and hydrolysis polymer, (b) the structure of a TSC microcapsule, (c) the process of fabrication microcapsules by TSC.

Fig. 1 illustrates the complex TSC process for forming the microcapsules. Fig. 1(a) depicts the chemical structure of styrene-maleic anhydride (SMA) and hydrolysis polymer. As a kind of polymer dispersant, SMA molecules will be hydrolysis by NaOH and then the -COO group insert and directional arrange on oil droplet surface. In Fig. 1(b), hydrophilic groups of carboxyl arrange alternatively along the backbone chains of SMA molecules. When hydrolyzed SMA molecules are adsorbed at the interfaces of oil droplets, it is easy for the molecules to have such directional arrangement with hydrophobic groups oriented into oil droplet and hydrophilic groups out of oil droplet. This kind of molecular arrangement brings results in a relatively strong electron negative field on the surface of oil particles. Anionic polyelectrolyte hydrolyzed SMA has anionic carboxyl groups that can interact with positively charged MF-prepolymer below the ζ potential. The MF-prepolymer was affinities on these particulates by static. Then, the reaction of microencapsulation took place under acid and heat effect on the surface of oil particles of emulsion, which formed membrane of capsule in such a way. Fig. 1(c) shows the formation process of the TSC by another prepolymer (MF) addition at a slowly rate. Also, under the effect of heat the second coacervation will cross-linked to form another part of shells. That can be concluded that the twice-addition prepolymer and twice increasing-decreasing temperature courses lead to compact shells.

2.3 MicroPCMs in emulsion

In order to bring the coacervation process to a clear understanding, optical microphotographs of microcapsules were taken to illuminate the details. Fig. 2 (a-b) show optical microphotographs of core material dispersed by hydrolyzed SMA after 5 min and 10 min at room temperature. At the beginning 5 min, the hye size distribution of drolyzed SMA dispersed the core material into particles. However, these particles had not been separated each other directly due to the molecule linkage of the hydrolyzed SMA. Being emulsified for 10 min, the core particles were separated through the regulation of hydrolyzed SMA molecules.

In previous study [12], we have drawn a conclusion that the average diameter of $1\mu\text{m}$ - $5\mu\text{m}$, fabricated under stirring speed of $3000\text{ r}\cdot\text{min}^{-1}$, is the perfect range of size insuring both of narrow size distribution and enough rigidity. Based on the experiment, MF prepolymer (32 g) was dropped into the above emulsion with a stirring speed of $3000\text{ r}\cdot\text{min}^{-1}$. The prepolymer cured on core particles in 60 min by increasing the temperature to $60\text{ }^{\circ}\text{C}$ slowly at a rate of $2\text{ }^{\circ}\text{C}\cdot\text{min}^{-1}$. Fig. 2(c) shows the optical microphotographs of microcapsules with fleecy or pinpoint morphologies. Imaginably, these incompact structures may lead cracking or releasing of core material such as Fig. 2 (d) showing.

Compared with OSC microcapsules, Fig. 2(e) shows the optical microphotograph of TSC ones. The prepolymer covered on particles without cracks and thparticles is uniform with global and distinct shape. Moreover, there is nearly no conglutination between each microcapsule in very stability solution system.

2.4 SEM morphologies of shells

Fig. 3(a) shows SEM morphology of dried OSC microcapsules with the size of $1\text{-}5\text{ }\mu\text{m}$. These microcapsules have a rough morphology and a little polymer occupies the interspaces of microcapsules. It can be contributed to the unencapsulated core material and the uncovered shell material. Especially, the surfaces have many protrusions, which may be occurred by

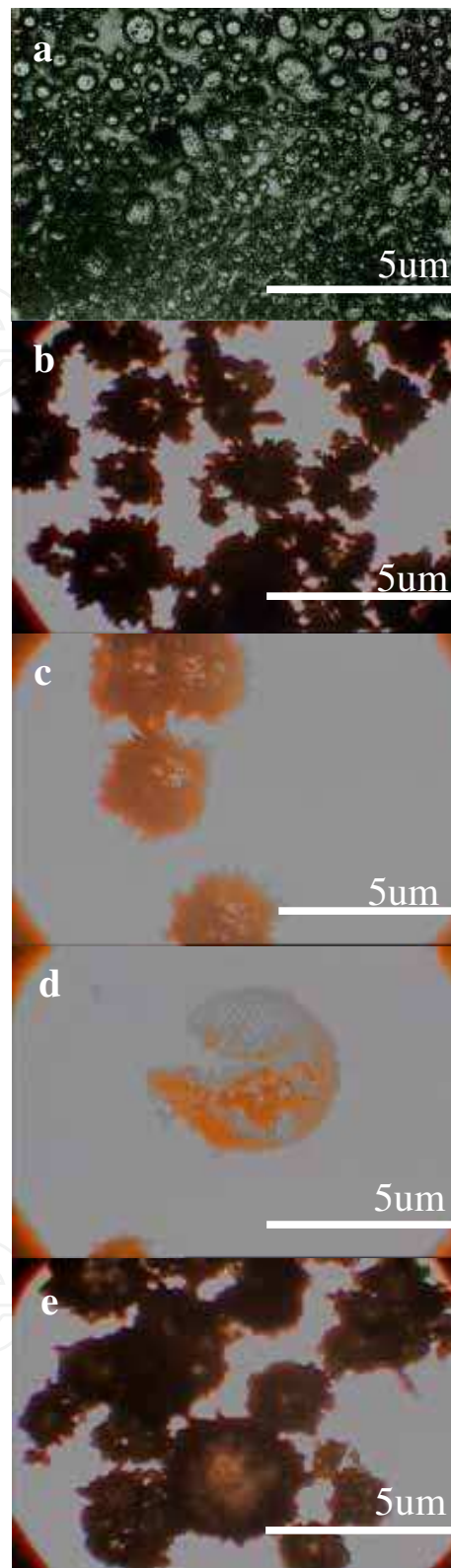


Fig. 2. Optical microphotographs of microcapsules: (a) core material dispersed by hydrolyzed SMA in water for 5 min; (b) core material dispersed by hydrolyzed SMA in water for 10 min; (c) microcapsules by OSC; (d) a crack OSC microcapsule (e) microcapsules by TSC.

not completely cross-linking or high-speed chemical reaction. In images Fig. 3(b-c) ($\times 10000$), it is clearly that the surfaces of microcapsules seem to be coarse and porous. Interestingly, there is a depressed center on a microcapsule reflecting the lower rigidity of shell in Fig. 3(d). We may draw a conclusion from these defects that OSC could not achieve a perfect coacervation on cores slowly and tightly in enough time under condition of mass shell material. Fig. 3(e) reflects the surface morphologies of piled microcapsules fabricated by TSC. It appears that nearly all these smooth microcapsules have a diameter about $2\ \mu\text{m}$ with regularly globe shape. Moreover, not only there is nearly no concavo-convex and wrinkle in bedded in shell surfaces, but also little polymer is pilling between piled microcapsules. From these results, it could be imaged that the method of twice-dropping prepolymer has decreased the roughage through molecules regulation of the second-dropped polymer. At the same time, the flaws may be decreased by padding the second cross-linking on the previous coacervation.

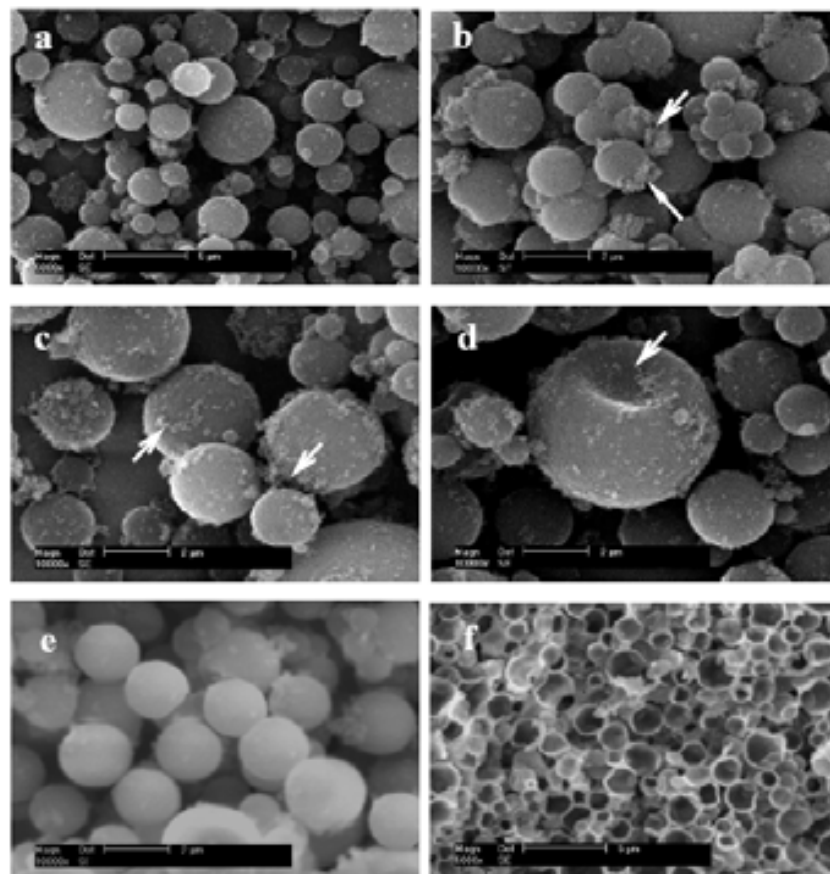


Fig. 3. SEM photographs of microcapsules dried in a vacuum oven at $40\ ^\circ\text{C}$ for 24 h, (a) (b) surface morphology of piled OSC microcapsules, (c) (d) the rough surface morphology of OSC microcapsules, (e) surface morphology of piled TSC microcapsules, (f) cross section of TSC microcapsules.

2.5 Density and thickness of shells

Density and thickness of shells are useful parameters reflecting the compactness of shells. Originally, the thickness data can be measured from cross-section of SEM images as shown in Fig. 3(f). In this study, a series of microcapsules were fabricated with various weight ratios of

core (32 g) and shell materials from 1.0 to 2.0 (core: shell) by two kinds of coacervation methods to evaluate encapsulation effect. All the microcapsules had the same preparation materials and environmental conditions. At least of fifty shells for each sample were measured and the average data was recorded by a MiVnt Image analyze system automatically.

From the data in Fig. 4(a), it shows that the thickness of OSC and TSC shells are both decreased with the increasing of value of weight ratios. And at the same weight ratios, all the thickness of TSC shell is less than that of OSC. This may be attributed to two aspects. Firstly, the TSC may decrease the structure defects, such as holes and caves. Secondly, this method of TSC allows the prepolymer to regulate their molecules on core material with enough reaction time for higher cross-linking density.

The data of density affected by various weight ratios are shown in Fig. 4(b). At the same weight ratio of 1.0, the densities of OSC and TSC are 1.75 g/cm³ and 1.67g/cm³, respectively. With the increasing of weight ratio, both densities of OSC and TSC shells are decreased. And at the weight ratio point of 2.0, both kinds of microcapsules have nearly shell density of 1.58 g/cm³.

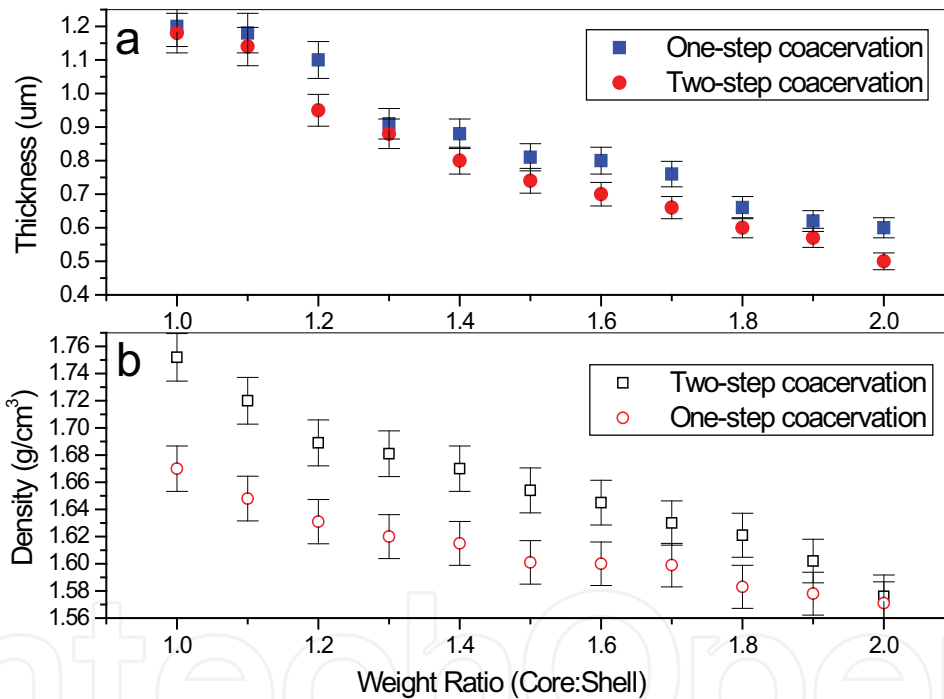


Fig. 4. The Data of shell thickness and density fabricated by OSC and TSC with various core and shell weight ratio.

2.6 Shell stability in water

Usually, we may simply evaluate the compactability and stability of shell by observing the morphologic changes of shell in water during different times. This method will be helpful to understand the structures of shells. In this study, dried microcapsules with diameter of 1µm were applied for convenience to indicate the endurance of shells in water by means of TEM. Fig. 5 (a-b) show the dried OSC microcapsules after immersed in water for 60 min and 120 min respectively. It is found clearly that the microcapsules are not spherical in shape because of absorbing water. And after 150 min, the polymer shell peeled off from the core

particles as shown in Fig. 5(c). The peeled shells are in spreading state and the core material has been separated without covering. We show particular interest to Fig. 5(d) depicting the compact TSC microcapsules after immersed in water for 150 min. Not only the capsules still keep the original global sphere and size nearly without peeling and expansion, but also the core material is safely protected avoiding releasing.

By referring back to Fig. 2 and Fig. 3, these above results are understandable in view of molecular structure of shells. When hydrolyzed SMA molecules were absorbed at the interfaces of the oil particles, the molecules had directional arrangement with hydrophobic groups oriented into oil droplet. It was easy for water to permeate in the shells through cracks and capillary. The force of interface adhesion between core and shell would reduce due to the static electricity force decreased by the effect of water molecular. Then, OSC microcapsules were swelled and destroyed with the time prolongation. Comparatively, shell of TSC microPCMs had less cracks and capillary, which also decreased the effect of water molecular.

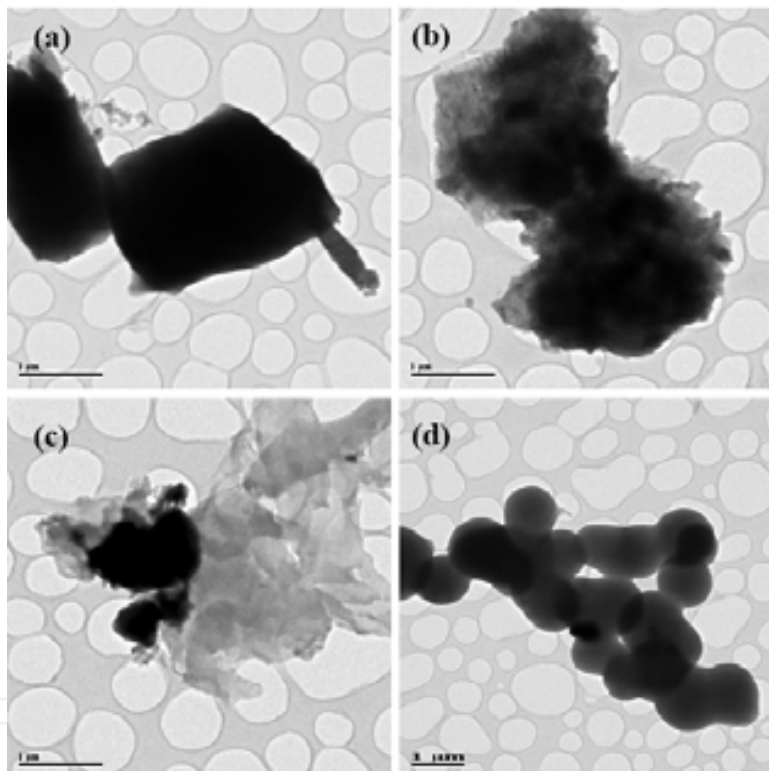


Fig. 5. TEM photographs of microcapsules in water, (a) OSC microcapsules in water for 30 min, (b) OSC microcapsules in water for 60 min, (c) OSC microcapsules in water for 90 min, (d) TSC microcapsules in water for 90 min.

2.7 Thermal stability of microcapsules

Fig. 6 shows thermogravimetric (TGA/DTG) curves of microcapsules prepared during various coacervation times. The blue and red lines are curves of TGA and DTG curves. Both axis of left and right are residual weight (%) of TGA curves and lose weight ratio of DTG curves. The microcapsules were decomposed with increasing temperature according to presenting residual weight (%). The curves may reflect thermal stability and structure of polymeric shell. Fig. 6 (a) shows that pure n-octadecane lost its weight at the beginning

temperature of 137 °C and lost weight completely at 207 °C. In order to know the compactness of encapsulation effect, we compare TGA curves of the OSC microcapsules fabricated by prepolymer dropping rates of 0.5 ml·min⁻¹ (Fig. 6b) and 1.0 ml·min⁻¹ (Fig. 6c). Contrastively, both kinds of OSC microcapsules containing *n*-octadecane lost weight rapidly at the temperature of 100 °C. The lost weight in the beginning may be some water and other molecule ingredients. And then the weight decreased sharply from 160 to 350 °C because of the cracking of shells. The weight-loss speed of microcapsules was distinctly less than that of pure *n*-octadecane. Though it indicates that the OSC method can encapsulate the core material, we can draw a conclusion that the lower dropping speed of shell material has little effect on improving the shell compactness.

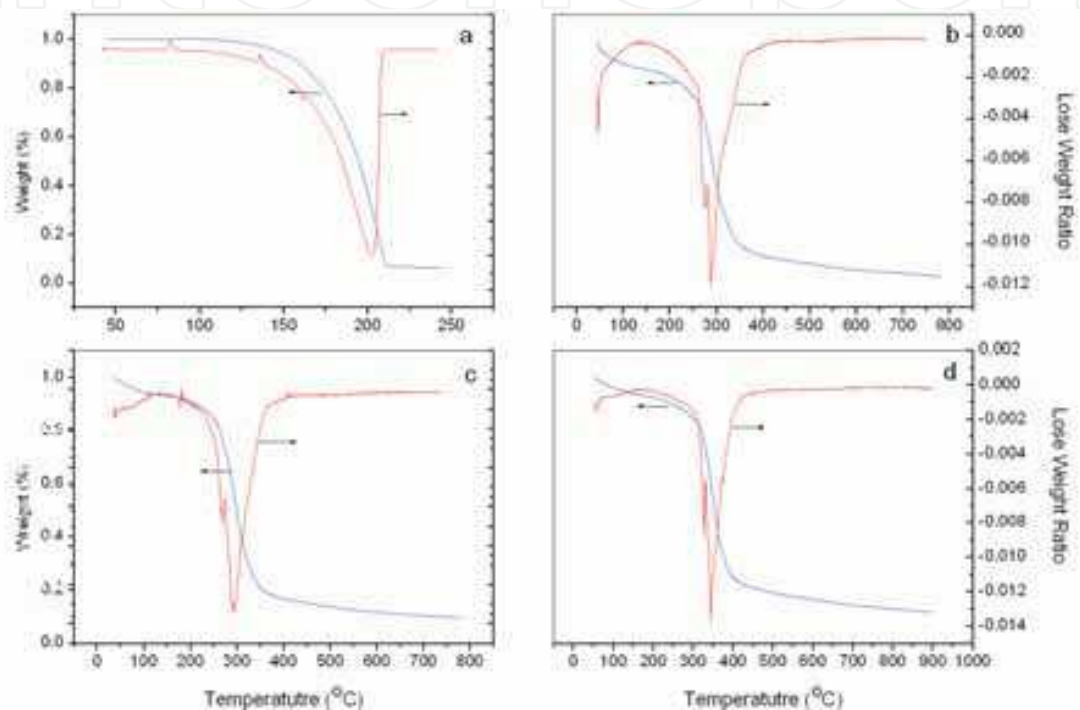


Fig. 6. TGA and DTG curves for (a) pure core material, (b) OSC microcapsules, (c) TSC microcapsules, made by 1.0 ml·min⁻¹ dropping rate of the second adding prepolymer, (d) TSC microcapsules, made by 0.5 ml·min⁻¹ dropping rate of the second adding prepolymer.

Fig. 6(d) shows TGA curve of the expected TSC microcapsules fabricated with dropping shell material speed of 0.5 ml·min⁻¹. It loses weight between 200 °C to 400 °C. We also find that the beginning temperature of TSC is higher than that of OSC, which proves that the method of TSC has a better effect on protecting of core material.

2.8 Permeability of microPCMs

Release rate depends largely on the polymer structure of shells, which in turn is influenced by the conditions employed in preparation. A typical SEM morphology of microcapsules after releasing is shown in Fig. 7. The arrows sign a broken shell-structure formed during releasing process. Moreover, the weight ratio of core and shell will greatly affect the permeability. For example, we have discussed that penetrability of microPCMs with average diameter 5 μm is lower than that of 1.5 μm. And their penetrability with mass ratio of 1:1 (core:shell) is lower than that of 3:1 and 5:1 under the same core material emulsion speed

[12]. Considering the above results, only one kind of microPCMs fabricated with mass ratio of 1:1 and diameter of 5 μm were selected in this study to simplify the relationship between the fabrication process and the permeability. In addition, there different shell-structures were fabricated by controlling of pre-polymer dropping speeds of 0.5, 1.0 and 2.0 $\text{ml}\cdot\text{min}^{-1}$, respectively.

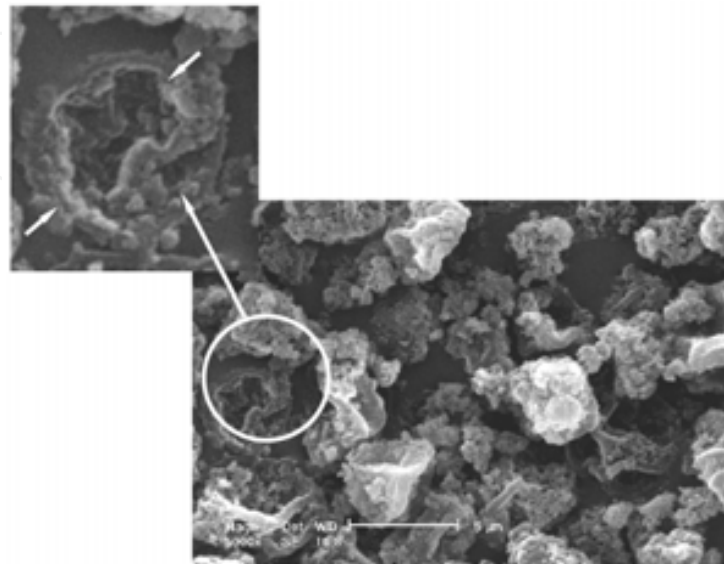


Fig. 7. A typical SEM morphology of broken microcapsules during releasing.

Fig. 8 shows curves of relationship between the percentage residual weight (wt. %) of core material in microcapsules and the time course of the transmittance. Five systems, coded as A-F, were measured in extraction solvent. The systems correspond to the following conditions of coacervation method and prepolymer dropping speed: A(■) OSC, 2.0 $\text{ml}\cdot\text{min}^{-1}$; B(●) OSC, 1.0 $\text{ml}\cdot\text{min}^{-1}$; C(▲) OSC, 0.5 $\text{ml}\cdot\text{min}^{-1}$; D(□) TSC, 2.0 $\text{ml}\cdot\text{min}^{-1}$; E(○) TSC, 1.0 $\text{ml}\cdot\text{min}^{-1}$ and F(Δ) TSC, 0.5 $\text{ml}\cdot\text{min}^{-1}$, respectively. Although the resultant microcapsules had been filtered and washed with water, there was a little un-encapsulated *n*-octadecane and other fabrication materials attaching on shells. Therefore, the initial transmittances in media are 98%, 98%, 98%, 97% and 99%, which were nearly equality values. The rate of permeation of OSC microcapsules shell decreases in the order of system A, B and C. It can be concluded that the shell pre-polymer dropping rates affect the penetrability directly. The total PCM permeated time from shells is just in 45 min of system A, comparing to 90 min of system B and 125 min of system C. Especially, the release profile of system A is directly just in one step, but systems of B and C have multi-steps. Comparatively, the rates of permeation of TSC microcapsules decrease in the order of system D, E and F with multi-steps. At the same time, the rate of permeation of TSC is all less than that of OSC even at same dropping rate. Moreover, the data in systems of D, E and F nearly do not change in the beginning 50 min, and system of F begins to change rapidly at the time of 90 min.

The reason of above-mentioned phenomena may be attributed to two aspects. One is that the pre-polymer concentration in solution determined by the dropping rate, will affects the shells formation speed. Under rapider dropping rate, the shell will be formed faster with enough shell material, which brings disfigurements, such as micro-crack, micro-cavity and

capillary on shells. These disfigurements will lead the core material to penetrate with low resistance. Contrarily, shells will form slowly under the situation of low pre-polymer concentration in solution. The pre-polymer molecules will adhere on core particles compactly. On the other hand, the channels and disfigurements of penetration in shells were decreased by the twice-dropping fabrication method. The core material penetrates the TSC shells need longer distance and more time. Thus, system of F presents the best resistance of core material.

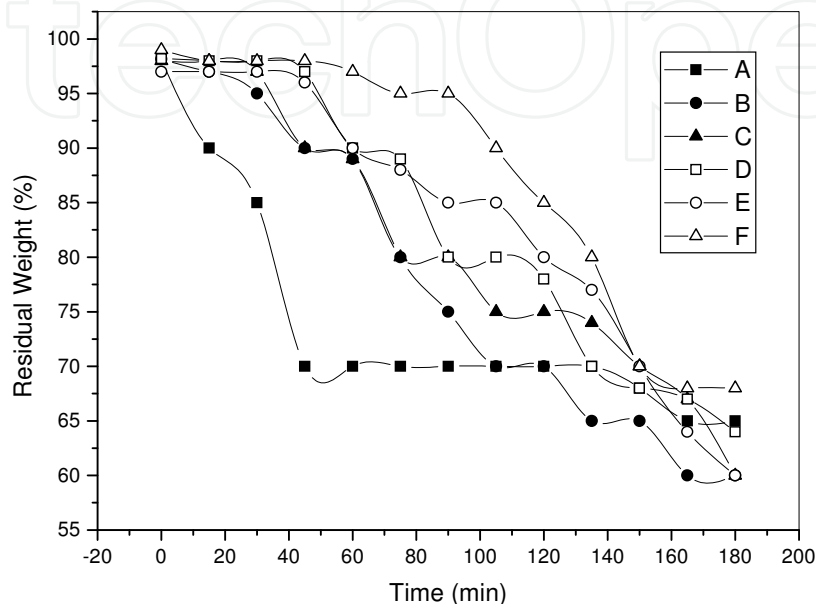


Fig. 8. Curves of the percentage residual weight (%) of core material in microcapsules in extraction solvent. The systems correspond to the conditions of coacervation methods and prepolymer dropping speed: A (■) OSC, 2.0 ml·min⁻¹; B (●) OSC, 1.0 ml·min⁻¹; C (▲) OSC, 0.5 ml·min⁻¹; D (□) TSC, 2.0 ml·min⁻¹; E (○) TSC, 1.0 ml·min⁻¹ and F (△) TSC, 0.5 ml·min⁻¹.

2.9 Permeability coefficient of the shell (k)

1ml of pure water suspension with the percentage weight of dried microPCMs being 10% was spread homogeneously with a wire bar on a polyethylene terephthalate (PET) film. Poly (vinyl alcohol) (PVA) played a role of a binder between the PET film and the microcapsules. The film was cut into squares of 1cm×1cm. The square films were soaked in to glass vessels containing 30 ml of ethyl alcohol with a density of 0.97 g ml⁻¹. The glass vessels were sealed avoiding volatility and with light stirring at a room temperature. The penetration property of different microcapsules was evaluated by an UV/visible spectrophotometry in ethyl alcohol. From changes of transmittance of light, we got the core material penetrating time and the residual weight (%) of core material. In this process, the optical density (OD) of the dispersing medium was measured and converted into the concentration of *n*-octadecane using a calibration curve,

$$\text{Residual weight (\%)} = \frac{OD_0 - OD_t}{OD_0} \times 100\% \quad (1)$$

where OD_0 is the optical density of all encapsulated core material in ethyl alcohol, OD_t is the optical density of encapsulated core material in ethyl alcohol at a permeation time (t).

Generally, the kinetic theory of penetrability is determined by the structure and characteristic of shell. Fundamentally, by comparing the permeability coefficient of the shells (k), the minimum can be chosen fabricated by different preparation processes. Most of release properties observed in experiments have been analyzed by kinetic theories based on Fick's Law with an assumption that the release rate is proportional to the concentration gradient of solutes [13, 14]. As each microcapsules system has different structure shell and core material, it is considered to be complex system [15] and required to employ different strict treatment to understand the release mechanism and to characterize such complex system clearly. In this study, we expect to get the compatible kinetic theory applied to the transfer of n-octadecane out of the TSC shell though the release curves of microcapsules in 20 wt. % ethanol.

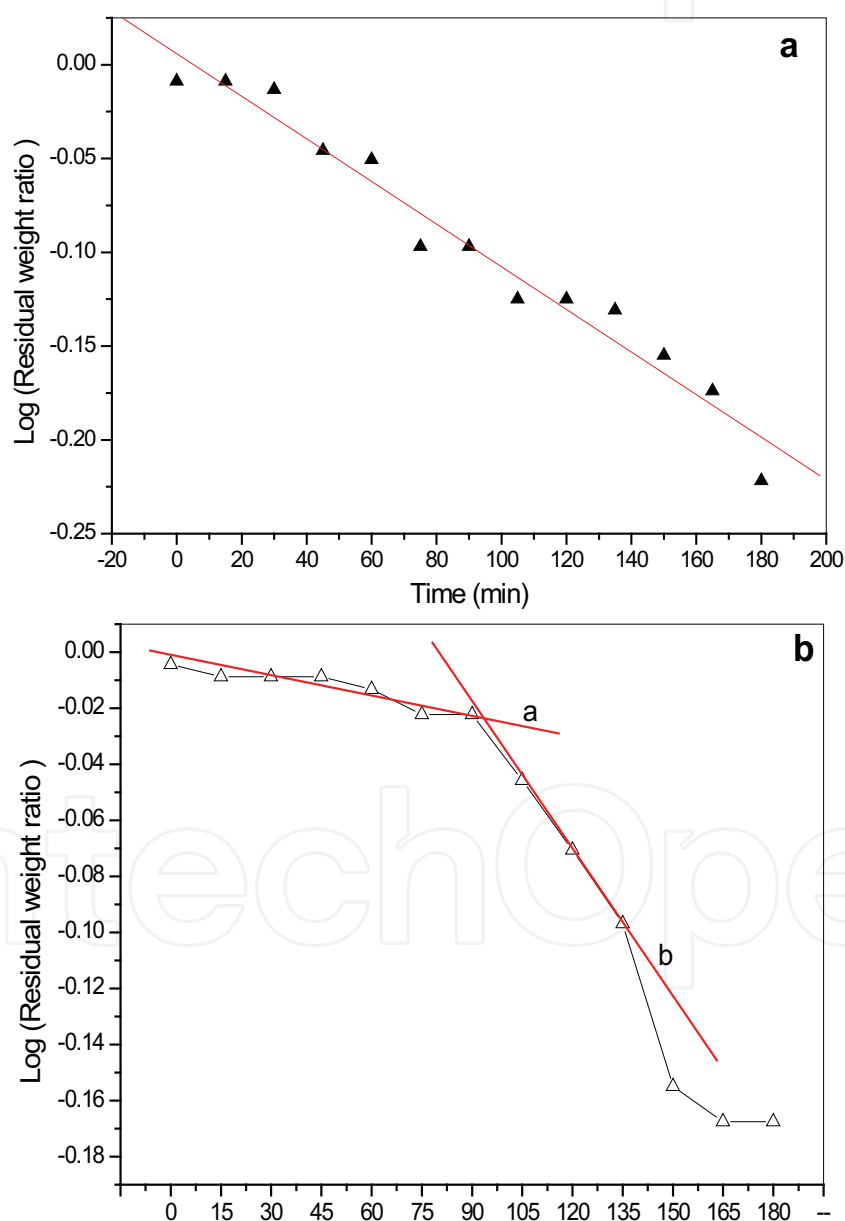


Fig. 9. The release curves of the OSC (a) and TSC (b) shells prepared by pre-polymer material dropping rates of $0.5 \text{ ml}\cdot\text{min}^{-1}$.

Fig. 9 shows the release curves of systems of C and F. It is linear relationship between time and logarithmic residual weight of core of system C in Fig. 9(a). Linear regression fit the first-order kinetic release theory,

$$2.303 \log q_{mc} / q_{\infty} = kt \quad (2)$$

where q_{mc} is the residual weight of core material at time t ; q_{∞} is the total weight of core material. The calculated value of k_1 is,

$$k_1 = -2.625 \times 10^{-3} \quad (3)$$

Fig. 9(b) shows the release curve of system F with a two decrease-linear step (line a and b) after curve regression. Lines of a and b separate at the release time of 90 min and the release rate of first step is lower than that of the second step. The TSC shell release curve of n -octadecane has a special release behavior, which reflects a complex shell structure. According to calculation of equation (3), the values of k_2 and k_3 are,

$$k_2 = -3.333 \times 10^{-4} \quad (4)$$

$$k_3 = -5.8333 \times 10^{-4} \quad (5)$$

By comparing the values of k_1 , k_2 and k_3 , it shows

$$k_1 > k_2 > k_3 \quad (6)$$

3. Fabrication and characterization MMF-shell microPCMs

To date, microPCMs/polymer composites have been paid more attention applying their thermo-regulation or thermo-saving abilities. A survey of literature shows that these composites are smart functional materials, such as thermosmart fibers, heat preservation building materials, solar heating materials and anti-icing coating, et al [16-19]. Although lots of investigations have been carried out, these composites have not yet been explored to a significant extent. Nearly all researches focused on the themes of selecting of PCMs, encapsulation methods, microPCMs characterization and thermal properties. However, we still have little knowledge about the interfacial morphology changes between microPCMs and matrix polymers, which will greatly affect the stability of microPCMs. Fig. 10 illustrates the mechanism of the interfacial morphology changes between microPCMs and matrix polymer. During a repeated phase change process with heat transmittance in application for microPCMs/polymer composites, expansibility will appear coming from both of microcapsules and polymeric resin with different inflation coefficients. The volume of microPCMs can be affected by the encapsulated PCM when environmental temperature changes. Moreover, the above phenomena may occur micro-cracks or fractures in matrix resin during heat absorbing and resealing; then these structures may spoil the thin shells of microcapsule (broken or ruptured), the encapsulated PCM will lose the shells protection [20]. Hence, the mechanical properties of composites will decrease following with the internal cracks or microcapsules rupture [21].

These entire interface changes certainly influence and shorten the service-life of these microPCMs/polymer composites [1].

It can be imaged from Fig. 10 that the encapsulated PCMs characteristics, microPCMs shell properties (thickness, intension and average diameter), matrix and the interfacial adhesion structures (microPCMs and matrix) are four main factors affecting the interfacial stability of microPCMs/polymer composites. To simplify this complex problem in this study, the shell property could be regarded as the only one characteristic being considered because of the microPCMs/polymer composites with the same shell and matrix materials. Normally, the microcapsule shell properties are determined by the weight ratios of core and shell materials and emulsification rates [22].

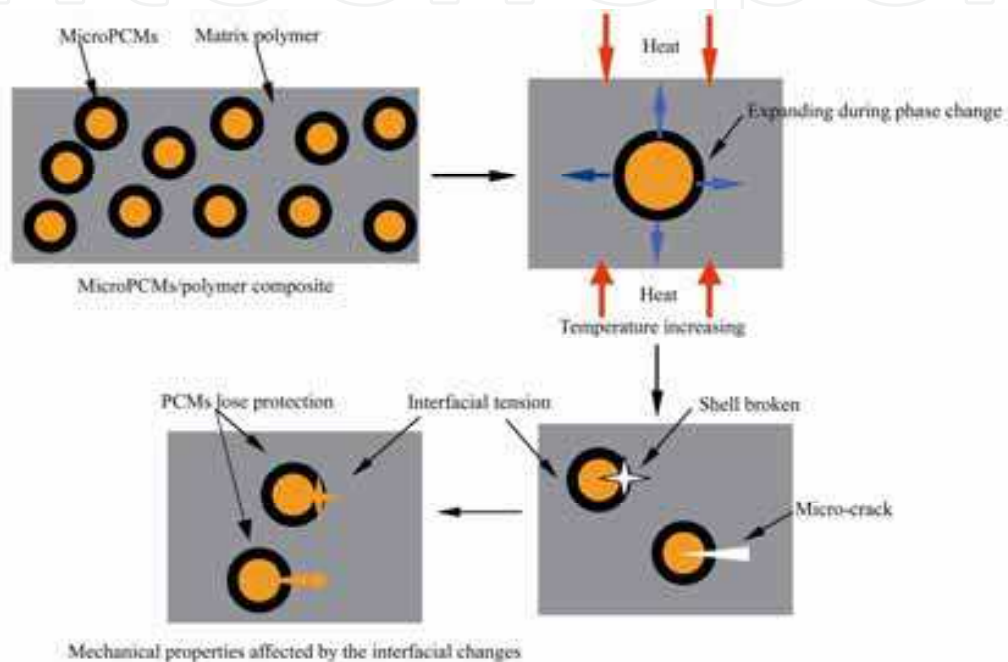


Fig. 10. Illustration of the mechanism of the interfacial morphologies changes between microPCMs and matrix polymers after repeated heat transmittance.

Based on these considerations, the purpose of this work was to fabricate novel microPCMs containing dodecanol by an in-situ polymerization using methanol-modified melamine-formaldehyde (MMF) as shell material and investigate the interfacial morphologies changes of microPCMs/epoxy composites treated with a simulant thermal process with a 10-times rapid temperature variation. A series of microPCMs with different core material (dodecanol) contents and diameters were prepared and embedded in epoxy resin to investigate the interfacial phenomena generated by the expansion or shrinking of the microPCMs during temperature change. Under this simulant and controlled thermal treatment conditions, the affects of average diameters and PCMs ratios of microPCMs on the interface morphologies of microPCMs/epoxy composite were analyzed applied the scanning electron microscopy (SEM). We believe these results will be guides for the fabrication and application of these functional composites.

3.1 Fabrication method

Dodecanol (Tianjin Kemel Chemical Reagent Development Center, Tianjin, China) was used as the PCM (core material). Its solid-liquid phase change temperature was about 21 °C. The

shell material was prepolymer of melamine-formaldehyde modified by methanol (Solid content was 78.0%, Aonisite Chemical Trade Co., Ltd., Tianjin). Styrene maleic anhydride (SMA) copolymer (Scripset® 520, USA) was applied as dispersant. Organic diluent (Butyl glycidyl ether), bisphenol-A epoxy resin (E-51) and curing agent (amine) were supplied by Tianjin Synthetic Material Research Institute (Tianjin, China).

The encapsulation was carried out in a 500 ml three-neck round-bottomed flask. 3.0 g SMA and 0.8 g NaOH were dissolved in 100 ml water (50 °C). The pH value was adjusted to 4-5 by acetic acid solution. 10.0 g dodecanol was added to the aqueous SMA solution, and the mixture was emulsified mechanically under a vigorous stirring rate of 3000 r min⁻¹ for 10 min using QSL high-speed disperse-machine (Shanghai Hongtai Ltd., Shanghai, China). Then dropped the emulsion in the bottle dipped in steady temperature flume and stirred at a speed of 1500 r min⁻¹, and dropped 25 g mixture of prepolymer (12.8 g) and deionized water at a rate of 0.25 g·min⁻¹. The shell formed after 2.5 h by heating slowly to temperature of 60 °C. After 30 min, the temperature was elevated to 75°C directly. After polymerization for 1.5 h, temperature was dropped slowly at 2 °C min⁻¹ to room temperature. The resultant microcapsules were filtered and washed with water and dried in a vacuum oven.

The 5 g of dodecanol microcapsules was mixed with 1.5 g organic diluent (Butyl glycidyl ether) by ultrasonic vibration for 5 min. The power of ultrasonic devices was 40 W. The 10 g bisphenol-A epoxy resin was dropped in the mixture prepared, and then the mixture was mixed by the same ultrasonic vibration for 5 min. 2.5 g of amine curing agent was added and ultrasonic vibrated for 5 min. At last, the mixture prepared was casted in the PTFE mold. After cured for 24 h at room temperature, the samples of were demoulded out.

3.2 FT-IR analyses of microPCMs synthetic structure

Fig. 11(a,b) illustrates the chemical structural formula of the MMF formation and the in-situ polymerization process of microcapsule shells. Melamine-formaldehyde (MF) microPCMs have been widely fabricated by in-situ polymerization because of their high mechanical properties and compactability of shells [22]. However, it is found that the MF shells have relatively high brittleness. This disadvantage may bring brittle broken of microPCMs under

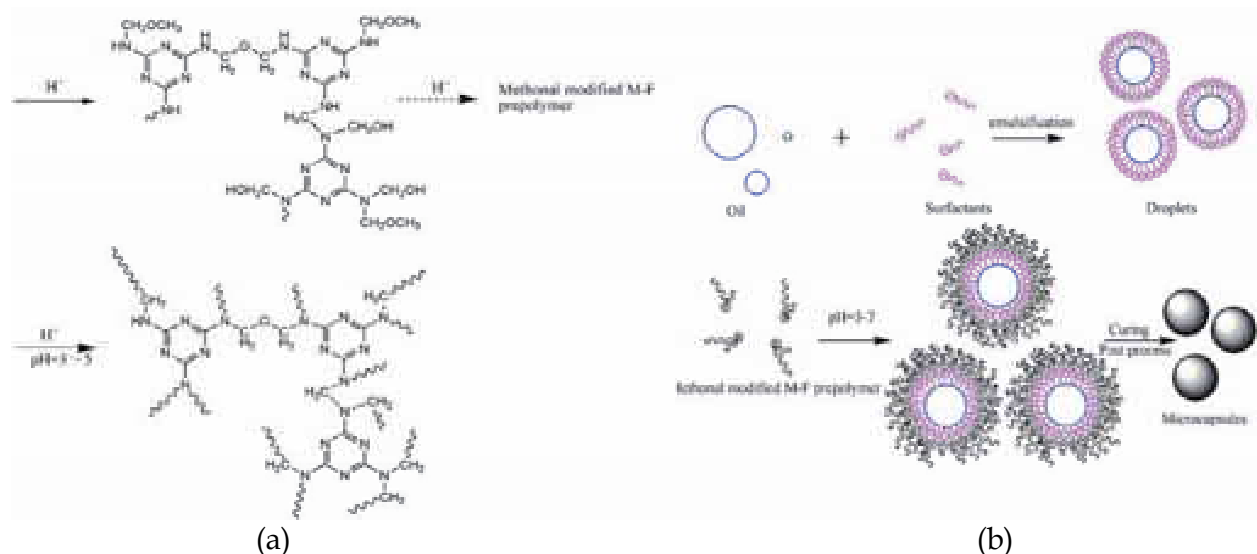


Fig. 11. Illustration of the (a) chemical structural formula of the MMF formation and (b) the in-situ polymerization process of microcapsule shells.

an extreme temperature change process or an impact force. The methanol groups were grafted on melamine with long branched structure to enhance the flexibility of MF-shells in this study (Fig. 11a). As Fig. 11b shown, the MMF shell formation is an in-situ polymerization process with the steps of W/O emulsification, MMF prepolymer adsorbed on oil particles and prepolymer polymerization. This method has been described in our previous report [20].

FT-IR could be applied to compare the chemical structures of MF and MMF shells, and to confirm the encapsulation of core material. Fig. 12 (a-e) shows the FT-IR spectra of (a) dodecanol, (b) SMA, (c) MMF, (d) MF and (e) microPCMs, respectively. The strong and wide absorption peaks at approximately 3369 cm^{-1} in Fig. 12 (a) of core material is assigned to O-H stretching vibrations of dodecanol. The multiple strong peaks at 2925 cm^{-1} and 2854 cm^{-1} are associated with aliphatic C-H stretching vibrations of methyl and methylene groups. The moderate strong peak at 1057 cm^{-1} is related to C-OH stretching vibration of primary alcohol. In Fig. 12(b), the peaks at approximately 1494 and 1603 cm^{-1} are assigned to the C=C stretching vibrations of benzene ring and the strong peaks at approximately 1858 and 1777 cm^{-1} are the C=O stretching vibrations of anhydride. In Fig. 12(c,d), the strong and wide absorption peaks at approximately 3342 and 3350 cm^{-1} are attributed to the superposition of O-H and N-H stretching vibrations. According to the work of Salaün [23], the peaks at 1556 and 815 cm^{-1} in Fig. 12. (c, d) are assigned to the vibrations of triazine ring; and the corresponding peaks of cured MMF lie at 1559 and 815 cm^{-1} . The characteristic peaks of aliphatic primary alcohol dodecanol at approximately 2925 , 2853 , and 1057 cm^{-1} can be observed in Fig. 12 (e) indicating that dodecanol has been microcapsulated with MMF resin. In addition, the characteristic peaks of MF resin at approximately 1550 and 814 cm^{-1} in Fig. 12 (e) indicates that dodecanol has been encapsulated as core material successfully with MF resin as shell material.

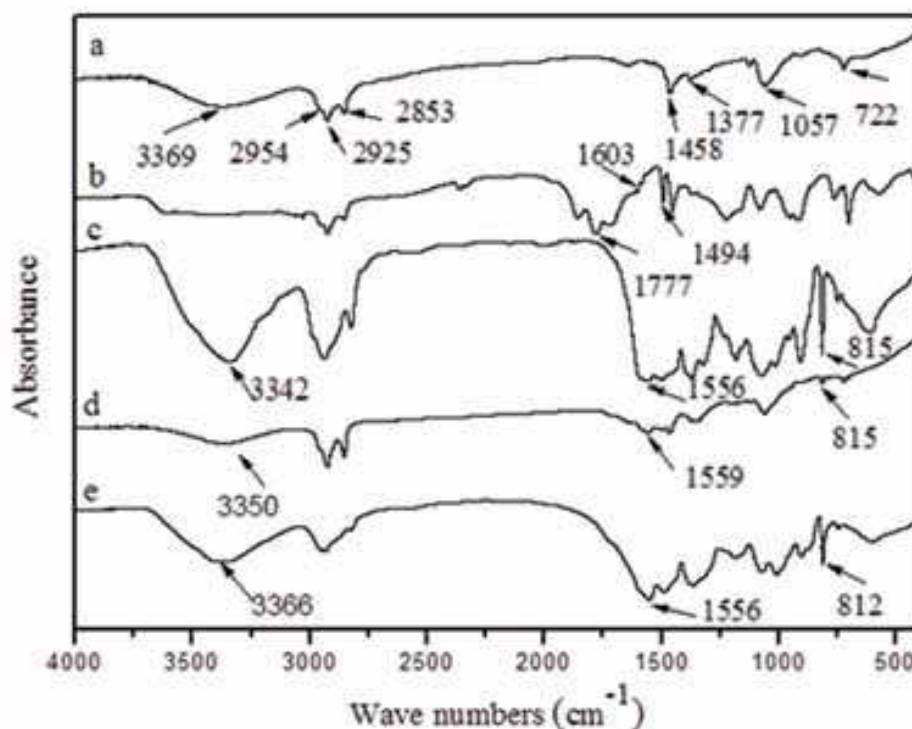


Fig. 12. FT-IR spectra of (a) dodecanol, (b) SMA, (c) MMF, (d) MF resin, (e) microPCMs.

3.3 Morphologies and average diameters of microPCMs

The contents of PCM in microcapsules can be estimated according to the Eq. (7) as the theoretical value (C_t , %),

$$C_t(\%) = \frac{m_{core}}{m_{core} + m_{shell}} \times 100\% \quad (7)$$

where m_{core} is the amount of core material (g) used and m_{shell} is the amount of shell material used (g) in synthesizing the microPCMs. The content of PCM in microcapsules (C_a , %) also can be estimated according to the measured melting heat according to Eq. (8),

$$C_a(\%) = \frac{|\Delta H_m|}{|\Delta H_{m_0}|} \times 100\% \quad (8)$$

$$E_e(\%) = \frac{C_a}{C_t} \times 100\% \quad (9)$$

where ΔH_m is the melting heat of microcapsules (J/g) and ΔH_{m_0} is the melting heat of PCM (J/g). The encapsulation efficiency (E_e , %) of microcapsules can be calculated as the ratio of the measured PCM content in microPCMs to the theoretical value depending on the amount of PCM and MMF prepolymer (Eq. 9) added in the system of fabrication.

The properties of microPCMs containing dodecanol synthesized by various conditions are listed in Tab. 1. The pure dodecanol has the melting enthalpy value of 206.9 J/g [24]. As the SMA amounts and stirring rates greatly affecting the microPCMs morphologies and properties [20], we firstly investigated the average diameter, C_a and E_e values of microPCMs fabricated by different C_t with the same string rate and the amount of SAM. The results show that the average diameter, C_a and E_e values have increased with the increasing of C_t . The average diameter is in the range of 1.55±0.84 to 1.99±1.10 μm, which is not greatly affected by C_t . Comparatively, the average diameter of microPCMs, fabricated with the same SAM amount (2.0 g) and C_t (50%) by different stirring rates (1000-4000 r min⁻¹), is in the range of 1.21±1.08 to 16.20±7.82 μm. With the increasing of stirring rates, the average diameters are sharply decreased. Interestingly, C_a and E_e values of microPCMs both increased with the increasing of stirring rates.

Samples (g)	SMhA amount	H ₂ O (g)	C _t (%)	Stirring rate (rmin ⁻¹)	Average diameter (μm)	Melting enthalpy (J/g)	C _a (%)	E _e (%)
Dodecanol	-	-	-	-	-	206.9	-	-
1	3.0	100	40.0	3,000	1.55±0.84	45.5	22.0	55.0
2	3.0	100	50.0	3,000	1.63±0.91	76.3	36.9	73.8
3	3.0	100	60.0	3,000	1.83±1.40	124.5	60.2	90.3
4	3.0	100	70.0	3,000	1.99±1.10	141.5	68.4	91.2
5	2.0	100	50.0	4,000	1.21±1.08	100.7	48.7	97.4
6	2.0	100	50.0	3,000	6.30±3.58	93.5	45.2	90.4
7	2.0	100	50.0	2,000	10.67±6.82	61.6	29.8	59.6
8	2.0	100	50.0	1,000	16.20±7.82	49.6	24.0	48.0

Table 1. Core contents and encapsulation efficiencies of microPCMs

Fig. 13 shows the SEM morphologies (a-d) and diameter number fractions (a'-d') of microPCMs fabricated with different C_t values (40, 50, 60 and 70%) under the same stirring rate of $3000 \text{ r} \cdot \text{min}^{-1}$. It can be seen that all the microcapsules have the irregular spherical shape. Some microPCMs are shrunken because of pressure or phase change. Their average diameter is about $1\text{-}2 \mu\text{m}$, and the different amounts of MMF have little affect on diameter of microPCMs. Fig. 14 shows the SEM morphologies (a-d) and diameter number fractions (a'-d') of microPCMs fabricated with different stirring rates (1000, 2000, 3000 and $4000 \text{ r} \cdot \text{min}^{-1}$; $C_t=50\%$). The average diameter was about $1.2 \mu\text{m}$ when the emulsification rate was $4000 \text{ r} \cdot \text{min}^{-1}$. With the increasing of stirring rates from 1000 to $4000 \text{ r} \cdot \text{min}^{-1}$, the average diameters decreased sharply. Also, some depressions on the surface of microcapsules were observed due to the liquid-solid phase change induced by the temperature decreasing in the process of synthesis of microcapsules.

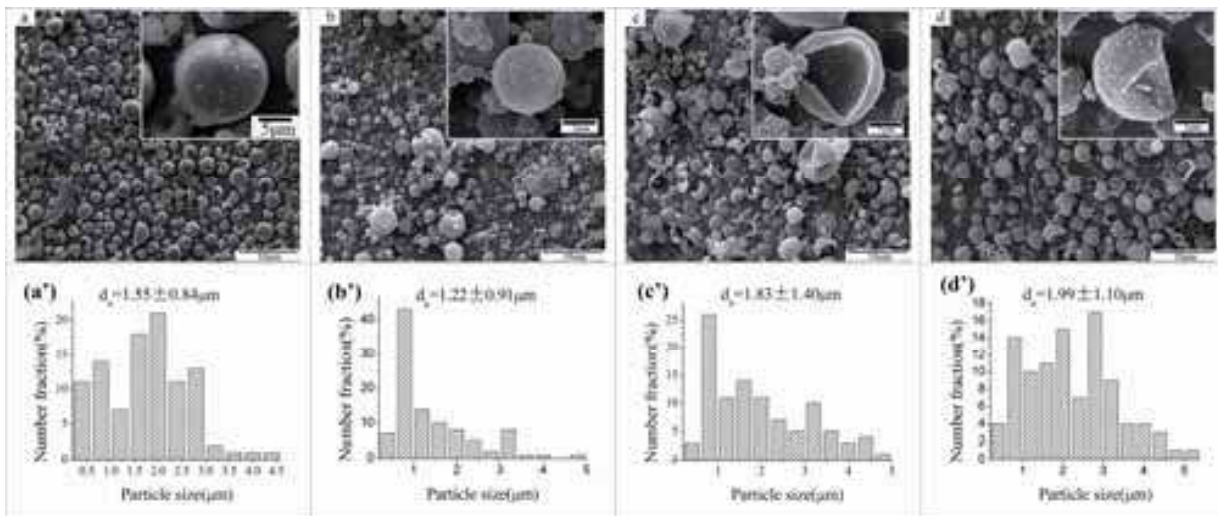


Fig. 13. SEM morphologies (a-d) and diameter number fractions (a'-d') of microPCMs fabricated with different C_t values (40, 50, 60 and 70%) under the same stirring rate of $3000 \text{ r} \cdot \text{min}^{-1}$.

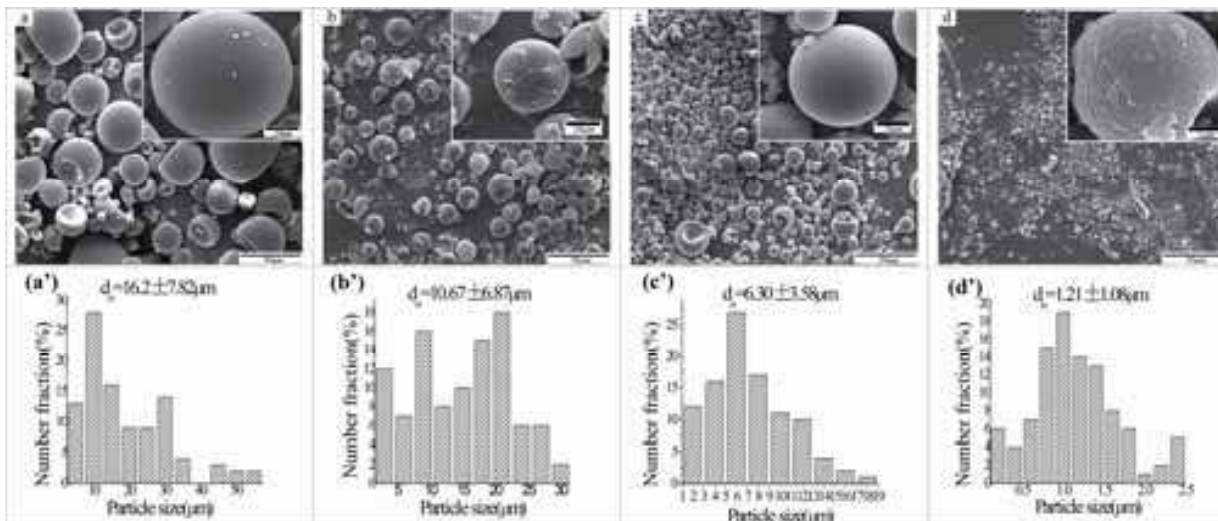


Fig. 14. SEM morphologies (a-d) and diameter number fractions (a'-d') of microPCMs fabricated with different stirring rates ($1000, 2000, 3000$ and $4000 \text{ r} \cdot \text{min}^{-1}$; $C_t=50\%$).

3.4 DSC analyses of microPCMs

Fig. 15 (a) shows the DSC curves (a-e) of pure dodecanol and the microPCMs synthesized with different C_t values of 40, 50, 60 and 70%. For pure PCM of dodecanol, the strongest endothermic peak at 24.3 °C is its phase change temperature. For each microPCMs sample, it has one obvious endothermic peak (curve b-e). With the C_t values increasing from 40 to 70% from microPCMs, their phase change temperatures are 20.9, 22.6, 23.5 and 24.3 °C, respectively. The shells of microPCMs do not greatly affect the phase change temperature of pure dodecanol.

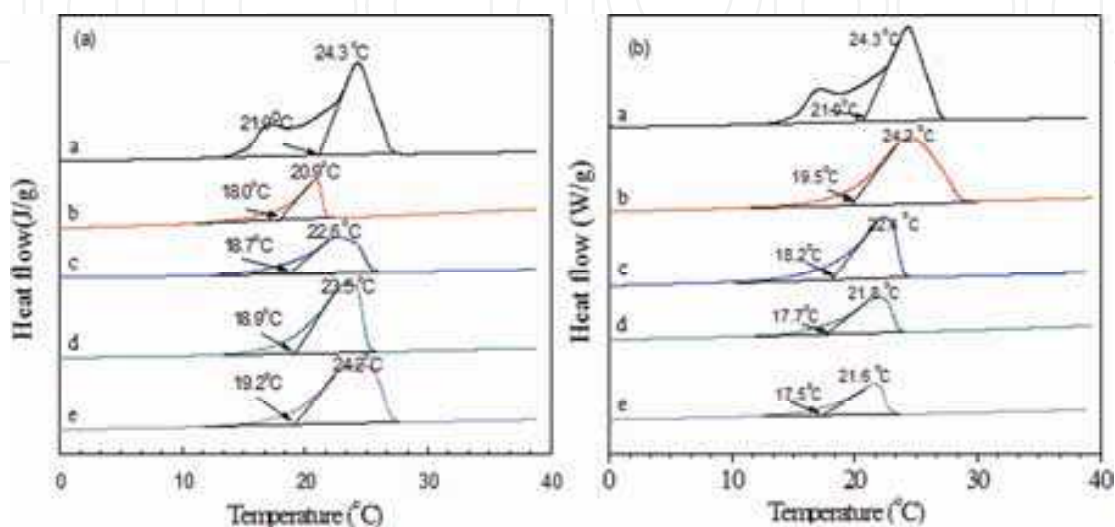


Fig. 15. DSC curves of (a) pure dodecanol and the microPCMs synthesized with different C_t values (40, 50, 60 and 70%); DSC curves of (b) pure dodecanol and the microcapsules synthesized with different stirring rates (1000-4000 r·min⁻¹; SMA=2.0 g, core/shell (wt/wt)=1/1).

In Fig. 15 (b), the phase change temperature and endothermic peak increased with increasing of emulsification rates for high core encapsulation because of better distribution of emulsifier in the emulsion system. The melting enthalpy and encapsulation efficiency (E_e , %) of dodecanol microcapsules synthesized at different conditions can be seen in Table 1. And the melting enthalpy and E_e were increasing with the increasing of C_t values and emulsification rates, which accorded with the DSC measurement results.

3.5 Interface morphologies of microPCMs/epoxy composites

A simulant temperature change process was designed in this study to lead the microPCMs in composites phase change. The temperature change was in the range of 15-50 °C, which could suffice the phase change of dodecanol. As the epoxy had the heat-resistance ability, this maximal temperature of this simulant process was higher than the phase change temperature of dodecanol. At the top temperature of 50 °C, the composites were retaining 10 min to ensure the absolute phase change of microPCMs. In order to evoke the interface variation distinctly, this temperature change process was fast (2 °C min⁻¹) and frequent (repeated 10 times). As C_t and the average diameter were two main parameters affecting the stability of microPCMs, we paid more attention to their effects on the interface morphologies of composites before and after the thermal treatments.

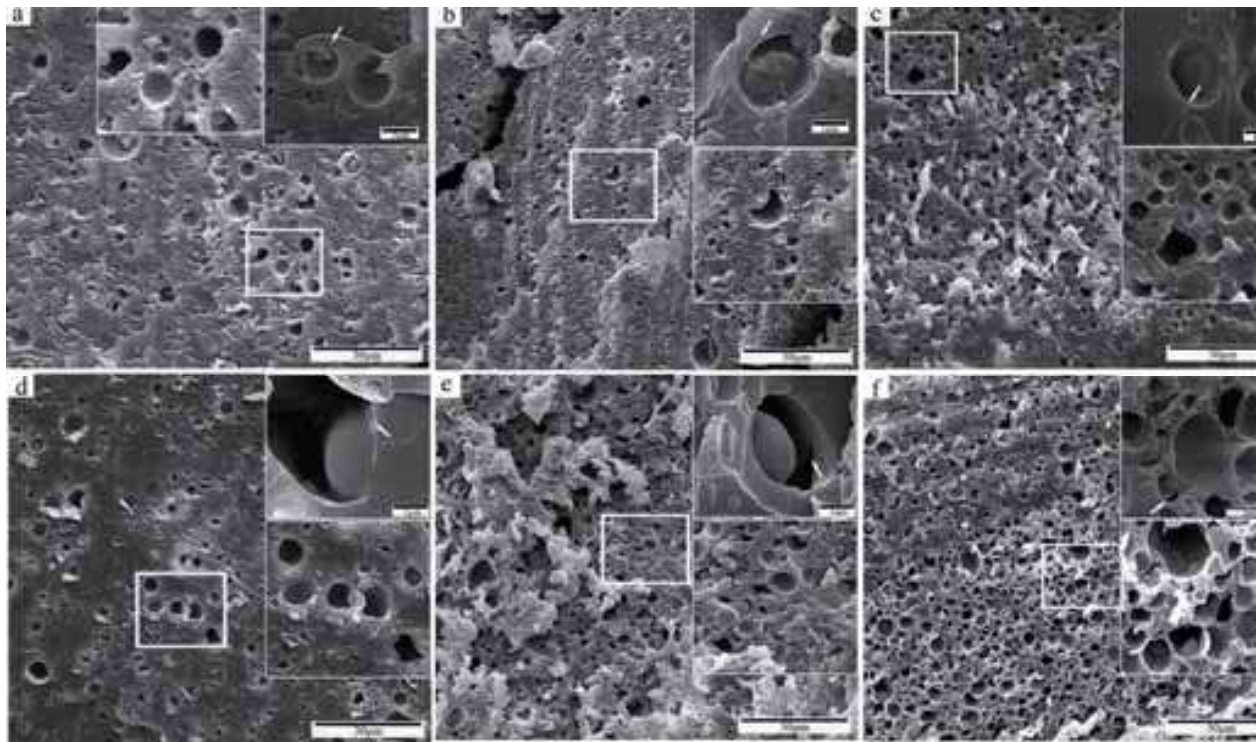


Fig. 16. SEM morphologies of microPCMs/epoxy composites (microPCMs/E-51, wt/wt=1/1) before (a, b, c) and after (d, e, f) a thermal treatment process with different C_t (%) values: (a) 40%, (b) 50%, (c) 60%.

Fig. 16 shows the SEM interface morphologies of microPCMs/epoxy composites (microPCMs/E-51, wt/wt=1/1) before (a, b, c) and after (d, e, f) the simultaneous thermal treatment process with different C_t (%) values: (a, d) 40%, (b, e) 50% and (c, f) 60%. All these morphologies indicate that the microPCMs could be dispersed homogeneously in epoxy resin through an ultrasonic vibration method. It would ensure the isotropic thermal transmission in composites. In Fig. 16 (a-c), more imbedded microPCMs will make the composites more loose. However, the interfaces of microPCMs/epoxy are compact without gaps. The shells of microPCMs and matrix adhere tightly keeping the microPCMs steadily. Comparatively, micro-cracks and gaps occurred after a thermal treatment in the interface of microPCMs and epoxy matrix obviously, as shown in Fig. 16 (d-f). With the increasing of C_t , the absorbing-releasing of latent heat will more intensively in composites. This will give great actions to interfaces between microPCMs and matrix polymers because of their different expand coefficients and thermal transmission abilities. At the same time, the inherent properties of volume expand for PCMs in tiny microcapsules induced the internal stress in the composites leading to separation of microPCMs and matrix. And the interface morphologies changes will be easily produced under the repeated expand-shrink affects and the internal stress actions.

Fig. 17 shows the SEM morphologies of microPCMs/epoxy composites (MicroPCMs/E-51, wt/wt=1/1; $C_t=50\%$) before (a, b, c) and after (d, e, f) a thermal treatment. These microPCMs had different average diameters fabricated by controlling the emulsion rates of 1000, 2000 and 3000 r min^{-1} , respectively. It can be seen from Fig. 17 (a-c) that higher stirring rate will make microPCMs with smaller average diameter, and the number of microPCMs will also increase with the accelerating of stirring. The interfaces of microPCMs/epoxy are also compact without gaps before the thermal treatment similar to the phenomena in Fig. 16 (a-c). In Fig. 17 (d), some

microPCMs are deformed under the repeated expand-shrink affects and the internal stress actions. The interface separation occurred between microPCMs and matrix as shown in Fig. 17 (e, f). Moreover, more micro-cracks appeared in the microPCMs/epoxy composites containing microPCMs fabricated with smaller average diameter.

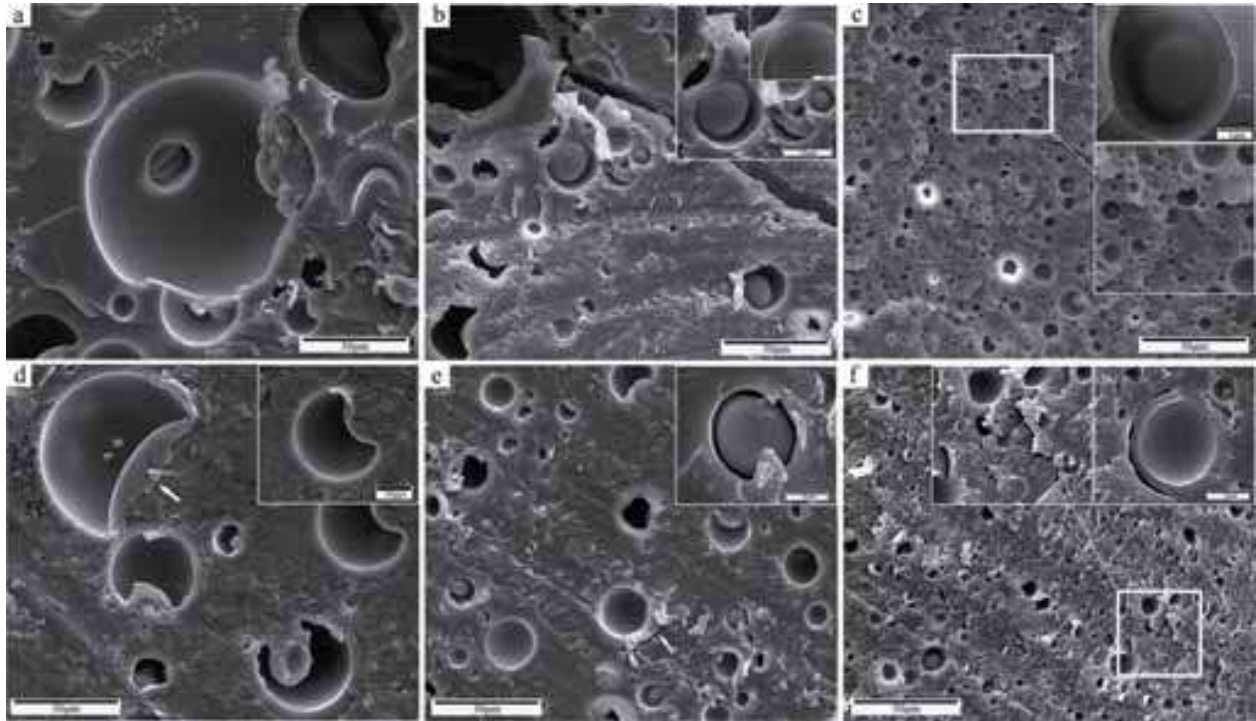


Fig. 17. SEM morphologies of microPCMs/epoxy composites (MicroPCMs/E-51, wt/wt=1/1; $C_t=50\%$) before (a, b, c) and after (d, e, f) thermal treatment containing microPCMs prepared by different emulsion rates: (a, d) 1000 r min^{-1} , $d_n=16.20 \pm 7.82 \mu\text{m}$; (b, e) 2000 r min^{-1} , $d_n=10.67 \pm 6.82 \mu\text{m}$; (c, f) 3000 r min^{-1} , $d_n=6.30 \pm 3.58 \mu\text{m}$.

Normally, both of C_t and the average diameter parameters will greatly affecting the shell thickness of microcapsules. Although the interface gaps or deformation of microPCMs had been detected in the composites treated with a thermal process (Fig. 16 and 17), there was no shell broken phenomenon for microPCMs embedded in matrix. The microPCMs with MMF shells have enough mechanical properties to resist the internal stress. It can be concluded that the internal stress generated by the expansion or shrinking of the microPCMs is the main factor leading to the interface morphology changes and damaged of composites. And these interface changes will affect the mechanical properties of these microPCMs/polymer composite in application. Therefore, these above results mean that we should balance C_t , the average diameter and mechanical properties of microPCMs/polymer composites systemically to satisfy the long service time of these composites.

4. Fabrication and characterization PU-shell microPCMs

A survey of literature indicates that melamine-formaldehyde (MF) resin, urea-formaldehyde (UF) resin and polyurethane (PU) are usually selected as microcapsule shell materials for the PCMs protection. However, there may exist ineluctable remnant formaldehyde after forming the shell through polymerization, such as using MF and UF resins, which causes environmental and health problems. Generally speaking, it is hard to find an effective

means to eliminate formaldehyde that is dissociative and can be continuously releasing from the products.

In this regard, PU is the promising polymer material in the field of microPCMs. Usually, a convenient technology is applied by polycondensating two complementary monomers to obtain PU-shell microcapsules. This method has been widely used in making flame-retarded, functional oil and artificial organ PU shell microcapsules [25–29]. It starts with making an emulsion of two immiscible phases (i. e., oil and water, O/W). Each phase contains a dissolved specific monomer that is able to react with the other monomer present in the other phase. In earlier studies of PU-shell microcapsules (TDI) [26], hexamethylene diisocyanate (HMDI) [30] and isophorone diisocyanate (IPDI) [31] are employed as the oil soluble monomers. In order to make the emulsion stable, certain surfactants or polymers are usually added to the continuous and/or the dispersed phase. Subsequently, these additives form an adsorption layer at the liquid–liquid interface, which may affect the polycondensation polymerization more or less [30]. After forming the nascent shell, the following polycondensation reaction is a diffusion-controlled process since it must occur at the O/W interfaces. As a result, capsule-like structured particles can be formed with the particle size depending on the initial emulsion conditions and formation process parameters, such as emulsion rate, reaction condition and molar ratio of monomers.

However, there was little information available focusing on the PU-shell microPCMs, especially relationship between properties and the dispersant, which is a main factor for stability and application of microPCMs. The aim of this research was to prepare a series of novel PU-shell microPCMs containing *n*-octadecane, which were fabricated by interfacial polycondensation between toluene-2, 4-diisocyanate (TDI) and diethylene triamine (DETA). *n*-Octadecane is usually a PCM desirable for usage in thermal storage and releasing for its availability in a reasonable phase change temperature range and its large amount latent heat [5]. The latent heat of *n*-octadecane is 241.2 J/g and its melting point (T_m) is 28 °C. Styrene-maleic anhydride copolymer solid (SMA) was used as a nonionic dispersant in this preparation. To investigate the effect of dispersant (SMA) on the properties of microPCMs is another focus point of this paper. Especially, in order to understand the thermal properties of microPCMs, the factors influencing thermal stability were examined with regard to the amount of SMA.

4.1 Fabrication method

The microcapsule shell was synthesized from TDI and DETA monomers, which were both purchased from Nankai University Special Reagent Co. for forming the microcapsule shell by using an interfacial polymerization process. *n*-octadecane (purity 98% minimum) was the core material as PCM purchased from Tianjin Chem. Reagent Co. Nonionic surfactant, SMA (Scripset®520, Hercules, USA) was used as a dispersant. All the chemicals were of reagent grade and used without further purification.

The concept of the microcapsules preparation method is based on the polycondensation reaction of hydrophilic and lipophilic monomers at the interface of an O/W submicronic emulsion. Initially, *n*-octadecane and lipophilic monomers TDI were dissolved in 20 ml of acetone as an oil phase. Different weight of SMA solid was dissolved in 40 ml of distilled water to adjusted pH value to 10 by using 0.1 M NaOH solution to form a serious microPCMs. The oil phase was then slowly dipped into the aqueous phase under magnetic stirring speed of 4000 r·min⁻¹ for 2 min. Then a measured DETA was diluted in 20 ml of distilled water, and then slowly added into the emulsion system to ignite the interfacial polycondensation. The microcapsules were formed by progressive interfacial

polycondensation reaction between DETA and TDI at the interface of hydrolysis SMA in water submicronic emulsion. After 2 h, the colloidal solution was then concentrated by evaporation under reduced pressure at 40 °C to about 20 ml.

4.2 Morphologies of PU-shell microPCMs

Fig. 18 shows the SEM morphologies of treated and dried microcapsules. In Fig. 18(a), the final microcapsules are found to be piled with a thickness of about 100 μm formed by deposition mechanism. It is very interestingly noted that the PU-shell microcapsules are individually distributed without excessive conglutination among each other. In Fig. 18(b), the surface of microcapsules is mostly smooth and the shape is regularly spherical with a diameter of about 5–10 μm . Some polymer filling between microcapsules can be observed, possibly due to that the core material could not have been encapsulated completely or the shell material could not absolutely cover the cores.

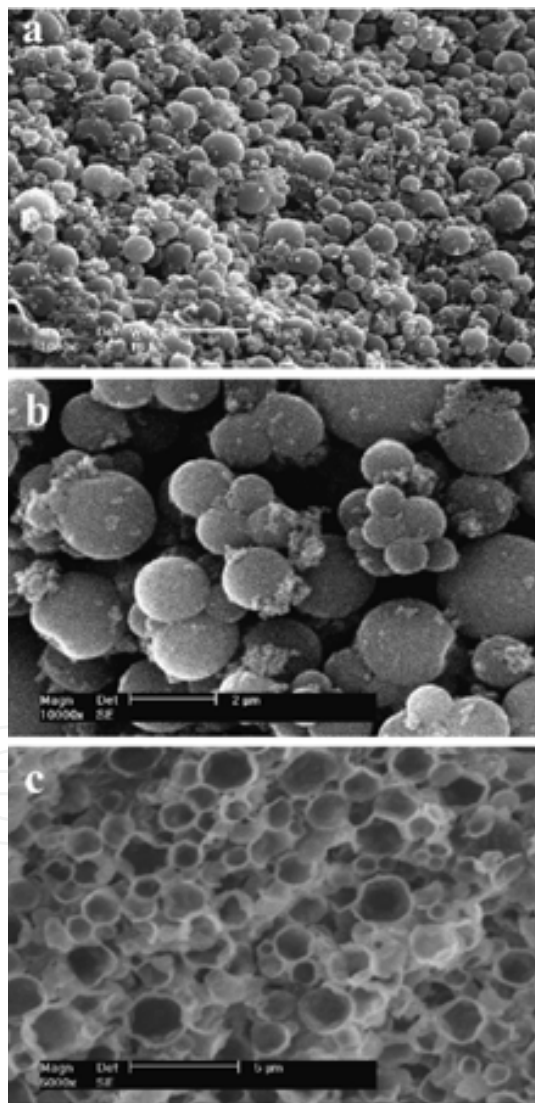


Fig. 18. SEM morphologies of treated and dried microcapsules: (a) piled microPCMs, (b) smooth and the regular global shape with a diameter of about 5–10 μm and (c) a typical cross-sectional morphology of shells.

In order to achieve the pure PU-shell material avoiding the influence of core material, the piled PU-shell microcapsules were blended in paraffin. After the blend was dried in room temperature, it was carefully cut to obtain the cross-section by an ultramicrotome (RMCMT-7000, USA). The half-shelled microcapsules were put into alcohol for removing PCM and paraffin. Then the shells were washed again with distilled water. In addition, it is very interesting that we can achieve the morphologies of the inside of the shell and the shell thickness after the pure shell material has been dried at 40 °C for 2 h. Fig. 18(c) shows the typical cross-sectional view of microcapsules. Obviously, it is seen that inside of the shell is rather smooth and the shell thickness is about 0.3–0.5 μm.

4.3 FTIR of shell material

FTIR analysis of shell material enables to determine the chemical structure of the shell polymer containing chemical bonds. Also, it will help us to understand the reality reaction degree of TDI. This information can be achieved from the core material in shells and the shell material. The liquid core material in shells at the temperature of 40 °C was separated from a half of the cross-section as abovementioned method by a centrifugal machine (Biofuge®Pico Barkey, Germany). The FTIR spectrum is shown in Fig. 19(a). It has absorption bands at 3367 and 1573–1542 cm⁻¹, which are assigned to the C–H stretching vibrations, C–H, CH₂ vibrations. The absorption bands at 2262 cm⁻¹ is the unreacted–NCO group coming from TDI. Fig. 19(b) shows an absorption band at 3471–3381 cm⁻¹ for the N–H stretching vibration, which may result in the formation of the strong hydrogen bonds on the shell side. C–H stretching vibrations of aliphatic diamine are shown at 2868, 1660 and 1726 cm⁻¹ for the C–O stretching of urethane. The sharp C–H stretching vibration for case (b) indicates that the SMA chain associated on core material may have reacted with TDI and formed a part of shell material. The chemical schematic is showed in Fig. 20. These FTIR results have confirmed that the shell of microcapsules is polyurethane.

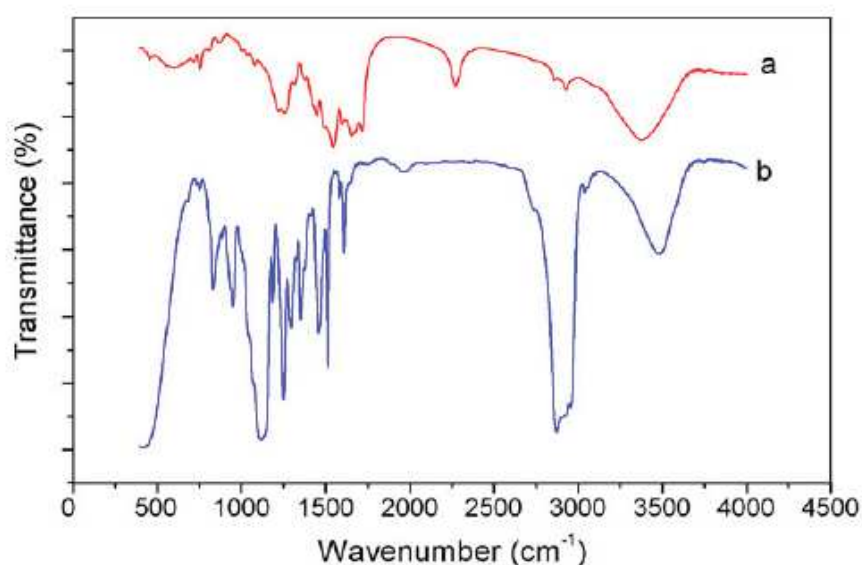


Fig. 19. FTIR curves of (a) liquid core material in shells and (b) shell material.

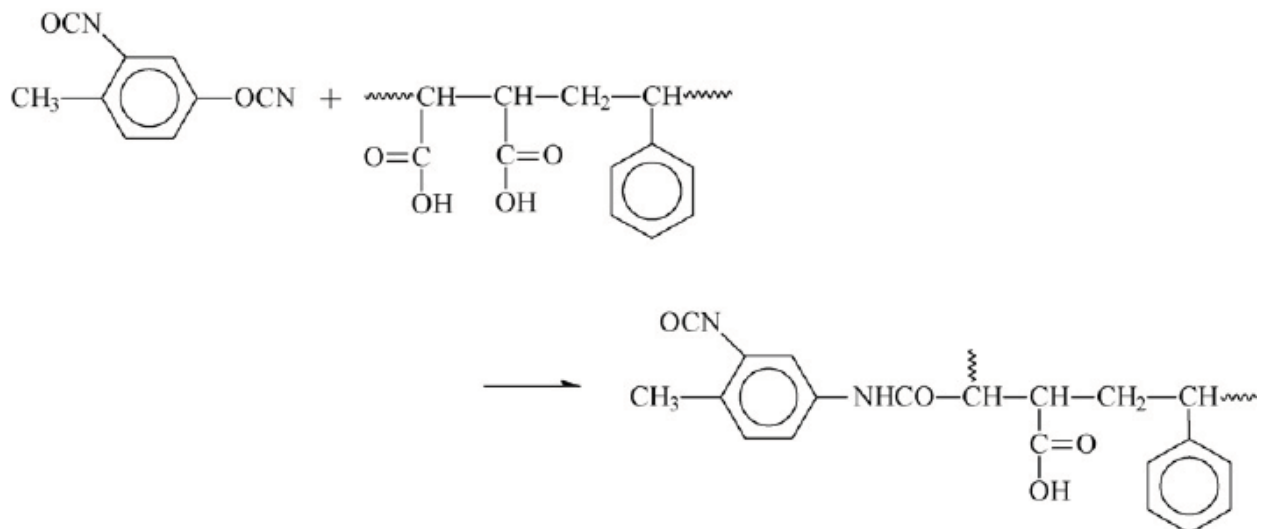


Fig. 20. The reaction scheme of SMA molecular and TDI.

5. Conclusions

1. In order to increase the compact properties of MF shell microPCMs containing *n*-octadecane, a method of TSC encapsulation through an in-situ polymerization was applied by dropping the shell material twice. All the evidences demonstrate that twice coacervations reduced the cracks and on shells and increase the compactness of shells. Especially, we confirm that the shell resistance permeability is increased by TSC shell technology from the values of permeability coefficient *k*.
2. MMF prepolymer can be applied as shell material to fabricate the microPCMs. The microPCMs containing dodecanol have the irregular spherical shapes and their average diameter can be controlled by regulating the stirring rates. The melting temperatures of these microPCMs were not greatly larger than the phase change temperature of pure dodecanol. With the increasing of stirring rates, the average diameters of microPCMs are sharply decreased. C_a and E_e values of microPCMs both increased with the increasing of stirring rates. As two main parameters affecting the stability of microPCMs, both C_t and the average diameter affected the interface morphologies of microPCMs/epoxy composites after the thermal treatments. Micro-cracks and gaps occurred after a thermal treatment in the interface of microPCMs and epoxy matrix obviously. The MMF-shells were flexible without broken. And the internal stress generated by the expansion or shrinking of the microPCMs is the main factor leading to the interface morphology changes and damaged of composites.
3. A series of PU-shell microPCMs containing *n*-octadecane is successfully prepared with particle size distribution properly controlled by the emulsion-stirring rate at

around 4000 r·min⁻¹. FTIR results have confirmed that the PU-shell microcapsules are successfully fabricated by interfacial polymerization between TDI and DETA with SMA as disperse.

6. Acknowledgements

The author is grateful to the financial support of the National Natural Science Foundation of China (No. 50803045).

7. References

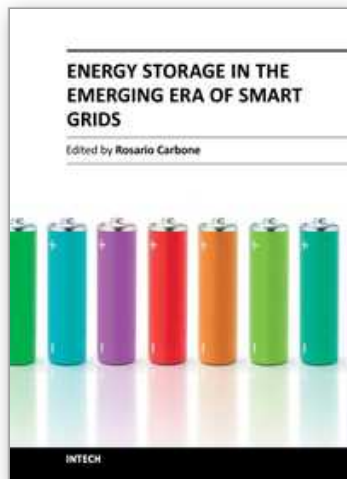
- [1] J. F. Su, L. X. Wang, L. Ren, Preparation and characterization of double-MF shell microPCMs used in building materials, *J. Appl. Polym. Sci.* 97(2005) 1755 - 1762.
- [2] M. N. A, Uddin M. S, Zhu H. J, Preparation and evaluation of a novel solar storage material: Microencapsulated paraffin, *Int. J. Solar Energy* 20 (2000) 227-238.
- [3] L. Y. Wang, P. S. Tsai, Y. M. Yang, Preparation of silica microspheres encapsulating phase-change material by sol-gel method in O/W emulsion, *J. Microencap.* 23 (2006) 3 -14.
- [4] X. X. Hu, Y. P. Zhang, Novel insight and numerical analysis of convective heat transfer enhancement with microencapsulated phase change material slurries: laminar flow in a circular tube with constant heat flux, *International J. Heat Mass Transfer* 45 (2002) 3163 - 3172.
- [5] X. X. Zhang, X. M. Tao, K. L. Yick, X. C. Wang, Structure and thermal stability of microencapsulated phase-change materials, *Colloid Polym. Sci.* 282 (2004) 330 - 336.
- [6] J. W. Kim, J. Y. Ko, J. B. Jun, I. S. Chang, H. H. Kang, K. D. Suh, Multihollow polymer microcapsules by water-in-oil-in-water emulsion polymerization: morphological study and entrapment characteristics, *Colloid Polym. Sci.* 281 (2003) 157-163.
- [7] K. Hong, S. Park, Preparation of polyurethane microcapsules with different soft segments and their characteristics, *React. Funct. Polym.* 42 (1999) 193-200.
- [8] X. X. Zhang, X. M. Tao, K. L. Yick, Y. F. Fan Expansion space and thermal stability of microencapsulated n-octadecane, *J. Appl. Polym. Sci.* 97 (2005) 390-396.
- [9] J. S. Hwang, J. N. Kim, Y. J. Wee, J. S. Yun, H. G. Jang, S. H. Kim, H. W. Ryu, Preparation and characterization of melamine-formaldehyde resin microcapsules containing fragrant oil, *Biotech. Bioprocess Engine.* 11 (2006) 332-336.
- [10] G. Sun, Z. Zhang, The mechanical properties of melamine-formaldehyde (M-F) microcapsules were studied using a micromanipulation technique, *J. Microencap.* 18 (2001)593-602.
- [11] Y. Rong, H. Z. Chen, D. C. Wei, J. Z. Sun, M. Wang, Microcapsules with compact membrane structure from gelatin and styrene-maleic anhydride copolymer by complex coacervation, *Colloids and Surfaces A: Physicochem.* 242 (2004) 17 - 20.
- [12] L. X. Wang, J. F. Su, L. Ren, Preparation of thermal energy storage microcapsules by phase change, *Polym. Mater. Sci. Engine.* 21 (2005) 276-279.
- [13] X. X. Zhang, X. C. Wang, X. M. Tao, K. L. Yick, Energy storage polymer/MicroPCMs blended chips and thermo-regulated fibers, *J. Mater. Sci.* 40 (2005) 3729-3734.

- [14] N. Nihant, C. Grandfils, R. Jerome, P. Teyssie, Microencapsulation by coacervation of poly(lactide-co-glycolide) IV. Effect of the processing parameters on coacervation and encapsulation, *J. Controlled Release* 35 (1995) 117-125.
- [15] K. Makino, M. Umetsu, Y. Goto, A. Kikuchi, Y. Sakurai, T. Okano, H. Ohshima, Two-Layer structure of microcapsule membrane as predicted from electrophoretic studies, *J. Colloid Interface Sci.* 218 (1999) 275-281.
- [16] P. Chaiyasat, Y. Ogino, T. Suzuki, M. Okubo Influence of water domain formed in hexadecane core inside cross-linked capsule particle on thermal properties for heat storage application. *Colloid Polym. Sci.* 286 (2008) 753-759.
- [17] H. Zhang, X. D. Wang, D. Wu. Silica encapsulation of n-octadecane via sol-gel process: A novel microencapsulated phase-change material with enhanced thermal conductivity and performance. *J. Colloid Interf. Sci.* 343 (2010) 246 - 255
- [18] C. Alkan, K. Kaya, A. Sara Preparation, Thermal Properties and Thermal Reliability of Form-Stable Paraffin/Polypropylene Composite for Thermal Energy Storage. *J. Polym. Environm.* 17 (2009) 254-258.
- [19] E. Onder, N. Sarier, E. Cimen. Encapsulation of phase change materials by complex coacervation to improve thermal performances of woven fabrics. *Thermochim Acta* 467 (2008) 63-72.
- [20] J. F. Su, L. Ren, L. X. Wang. Preparation and mechanical properties of thermal energy storage microcapsules. *Colloid Polym. Sci.* 284 (2005) 224-228.
- [21] M. You, X. X. Zhang, W. Li, X. C. Wang. Effects of MicroPCMs on the fabrication of MicroPCMs/polyurethane composite foams. *Thermochim Acta*, 472:(2008) 20-24.
- [22] J. F. Su, Z. Huang, L. Ren. High compact melamine-formaldehyde microPCMs containing n-octadecane fabricated by a two-step coacervation method. *Colloid Polym. Sci.* 285 (2007)1581-1591
- [23] F. Salaün, I. Vroman. Influence of core materials on thermal properties of melamine-formaldehyde microcapsules. *Eur. Polym. J.* 44 (2008) 849-860.
- [24] A. Abhat. Low temperature latent heat thermal energy storage. *Heat storage materials. Sol. Energy* 30 (1983) 313-332.
- [25] S. Giraud, S. Bourbigot, M. Rochery, I. Vroman, L. Tighzert, R. Delobel, F. Poutch, Flame retarded polyurea with microencapsulated ammonium phosphate for textile coating, *Polym. Degrad. Stab.* 88 (2005) 106-113.
- [26] K. Hong, S. Park, Characterization of ovalbumin-containing polyurethane microcapsules with different structures, *Polym. Test.* 19 (2000) 975-984.
- [27] O. Maruyama, T. Yamane, N. Tsunemoto, et al. , A preliminary study of microcapsule suspension for hemolysis evaluation of artificial organs, *Artif. Organs* 23 (1999) 274 - 279.
- [28] E. Jabbari, M. Khakpour, Morphology of and release behavior from porous polyurethane microspheres, *Biomaterials* 21 (2000) 2073-2079.
- [29] K. Hong, S. Park, Preparation of polyurea microcapsules with different composition ratios: structures and thermal properties, *Mater. Sci. Eng. A* 272 (1999) 418 - 421.
- [30] K. Mizuno, Y. Taguchi, The effect of the surfactant adsorption layer on the growth rate of the polyurethane capsule shell, *J. Chem. Eng. Jpn.* 38 (2005) 45 - 48.

- [31] L. Torini, J. F. Argillier, N. Zydowicz, Interfacial polycondensation encapsulation in miniemulsion, *Macromolecules* 38 (2005) 3225–3236.

IntechOpen

IntechOpen



Energy Storage in the Emerging Era of Smart Grids

Edited by Prof. Rosario Carbone

ISBN 978-953-307-269-2

Hard cover, 478 pages

Publisher InTech

Published online 22, September, 2011

Published in print edition September, 2011

Reliable, high-efficient and cost-effective energy storage systems can undoubtedly play a crucial role for a large-scale integration on power systems of the emerging “distributed generation” (DG) and for enabling the starting and the consolidation of the new era of so called smart-grids. A non exhaustive list of benefits of the energy storage properly located on modern power systems with DG could be as follows: it can increase voltage control, frequency control and stability of power systems, it can reduce outages, it can allow the reduction of spinning reserves to meet peak power demands, it can reduce congestion on the transmission and distributions grids, it can release the stored energy when energy is most needed and expensive, it can improve power quality or service reliability for customers with high value processes or critical operations and so on. The main goal of the book is to give a date overview on: (I) basic and well proven energy storage systems, (II) recent advances on technologies for improving the effectiveness of energy storage devices, (III) practical applications of energy storage, in the emerging era of smart grids.

How to reference

In order to correctly reference this scholarly work, feel free to copy and paste the following:

Jun-Feng Su (2011). Fabrication and Characterization of MicroPCMs, Energy Storage in the Emerging Era of Smart Grids, Prof. Rosario Carbone (Ed.), ISBN: 978-953-307-269-2, InTech, Available from:
<http://www.intechopen.com/books/energy-storage-in-the-emerging-era-of-smart-grids/fabrication-and-characterization-of-micropcms>

INTECH
open science | open minds

InTech Europe

University Campus STeP Ri
Slavka Krautzeka 83/A
51000 Rijeka, Croatia
Phone: +385 (51) 770 447
Fax: +385 (51) 686 166
www.intechopen.com

InTech China

Unit 405, Office Block, Hotel Equatorial Shanghai
No.65, Yan An Road (West), Shanghai, 200040, China
中国上海市延安西路65号上海国际贵都大饭店办公楼405单元
Phone: +86-21-62489820
Fax: +86-21-62489821

© 2011 The Author(s). Licensee IntechOpen. This chapter is distributed under the terms of the [Creative Commons Attribution-NonCommercial-ShareAlike-3.0 License](#), which permits use, distribution and reproduction for non-commercial purposes, provided the original is properly cited and derivative works building on this content are distributed under the same license.

IntechOpen

IntechOpen